Influence of weak binding and exotic structure in reaction with weakly bound nuclei near the Coulomb barrier

A. Shrivastava[1,*]

[1]*Nuclear Physics Division, Bhabha Atomic Research Centre, Mumbai - 400085, INDIA*

[*] *email: aradhana@barc.gov.in*

Recent measurements of fusion and direct reactions in case of weakly bound stable nuclei (^{6,7}Li) at extreme sub-barrier energies and the most neutron rich Borromean nucleus (^{8}He) at sub barrier energies using a new sensitive off beam technique are presented. The results illustrate role of low breakup thresholds and exotic structures on reaction dynamics. This along with study of capture reaction of the breakup fragments using particle- gamma coincidences is presented, thereby giving the current status of the field .

1. Introduction

The fusion of complex nuclei is governed by a delicate balance between the attractive nuclear and repulsive Coulomb interactions. During the last three decades of sub-barrier fusion studies, the important observations made are the discovery of sub-barrier fusion enhancement associated with couplings to the intrinsic excitations and nucleon transfer of the participating nuclei, measurements of the spin-distributions of the fused-compound nuclei and their theoretical description and the introduction of the concept of barrier distributions and their subsequent detailed measurements. Excellent reviews are given by Ref. [1]. Recently a new phenomenon of hindrance in fusion reactions has been reported in medium-heavy systems at deep sub barrier energies [2].

Low energy radio active ion beams available from ISOL facilities revived the field of sub-barrier fusion [3] and also generated new interest in measurements with weakly bound stable nuclei that are available in relatively high intensities. The differences in the reaction dynamics of well bound and weakly bound nuclei arise due to the presence of low-lying continuum, short-lived resonance states and low nucleon(s) separation energies in the latter [3]. This led to the expectation that breakup of the projectile would be a dominant channel to influence the reaction dynamics. Experiments with weakly bound stable nuclei incident on heavy target nuclei have demonstrated that the above-barrier fusion cross-sections are suppressed compared with the expectations for well-bound nuclei and a significant contribution of reaction products where part of the fragment is captured by the target [3,4]. On the other hand with short-lived radioactive ion beams (RIB) along with weak binding, unusual neutron or proton asymmetry and extended spatial distributions (halos), provide access to uncharted territories addressing fundamental questions of nuclear existence, multidimensional tunneling, pairing and cluster correlations. However measurements of fusion and transfer cross sections involving short-lived RIB around the Coulomb barrier are extremely restricted due to the required substantial increase in sensitivity [5,6] compared to stable beams.

In this presentation measurement of fusion cross-section and direct reactions in case of weakly bound stable nuclei using a new sensitive off beam technique will be discussed. First section deals with deep sub-barrier fusion measurement for ^{6}Li+^{198}Pt [7] to study phenomenon of fusion hindrance followed by study of sub-barrier fusion measurement with most neutron rich ^{8}He [6], to study breakup vs. nucleon transfer. Section 3 deals with the study of fragment capture reaction.

2. Exploring fusion at deep sub barrier with weakly bound ^{6}Li

In this section, we present a fusion measurement at deep sub-barrier energies for studying the phenomenon of fusion hindrance, in case of the weakly bound projectile ^{6}Li (alpha/t=1.45 MeV) [7]. Measurements with medium-heavy nuclei highlighted the change of

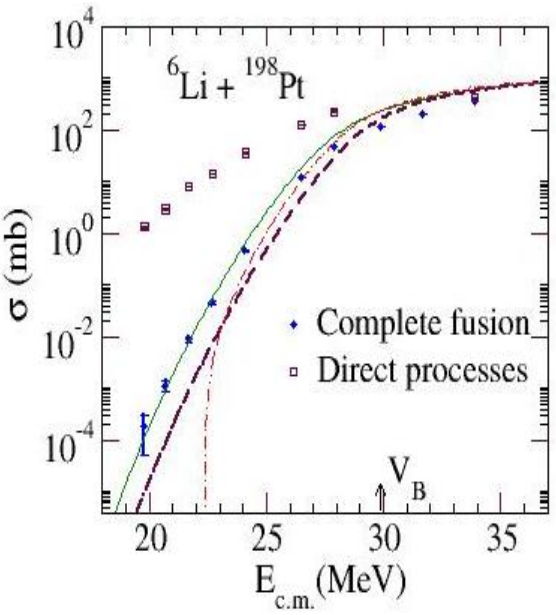

Fig.1 Cross sections for compound-nucleus formation and direct processes obtained from a sum of the partial cross sections. The results of the coupled-channels calculations using the WS potential (solid line), along with single-channel calculations using the WS potential (dashed line) and the M3Y potential with a repulsive core (dot-dashed line), are shown

slope of the fusion excitation function at deep sub-barrier energies compared to coupled channels calculations [2]. The energy where these deviations begin referred to as the threshold energy for observing fusion hindrance has been parameterized and its implications on the fusion with light nuclei of astrophysical relevance have been discussed [2]. Dasso and Pollarolo [8] pointed out that the cross-sections at deep sub-barrier energies could be used as an unique tool to obtain the value of the nuclear potential at small distances (see also [9]). More recently Ichikawa [10] showed that the potential energy at the touching point strongly correlates with this threshold energy. Micsicu and Esbensen proposed a potential with a shallow pocket (as compared to that obtained from Woods-Saxon parametrization) based on a sudden approximation, where the reaction takes place so rapidly that the colliding nuclei overlap with each other without changing their density [11]. A repulsive core included to take into account the nuclear compressibility arising due to Pauli Exclusion Principle, modifies the depth and the shape of the minima of the internuclear potential at small distances. They also showed that, depending on the choice of the couplings used in the calculations, there were surprising structures in the calculated average angular momentum at these low energies. The nucleus-nucleus interaction potentials extracted from the microscopic time-dependent Hartree-Fock theory indicate that at low energies the frozen density approximation breaks down underlying re-organization of the internal degrees of freedom Based on an adiabatic picture, a dynamical two-step model was proposed by Ichikawa et al. [10] to explain the deep sub-barrier fusion data. It should be noted that the above two approaches based on the sudden and adiabatic models predict different angular momentum distributions The measurement of the average angular momentum could also discriminate between the two approaches mentioned above that describe the fusion data equally well. In the sudden approach, using a shallow potential the average angular momentum of the compound nucleus is always smaller than in the two-step adiabatic model at low energies.

The fusion of weakly bound nuclei, which is a subject of current interest, has yet not been investigated at energies far below the barrier. For exotic weakly bound projectiles, a fully quantum mechanical time dependent wave-packet approach using a three body model also predicts a suppression of total fusion compared to corresponding stable nuclei over the entire energy range. Experimental studies at deep sub-barrier energies have been restricted mainly to the measurement of fusion cross-sections of symmetric systems [2] with the exception of ^{16}O + ^{204,208}Pb systems [12], spanning a range of ``stiffness", reduced mass. The possible effects that explain the change in slope of the measured fusion cross-sections are expected to be a general phenomenon. Hence measurements of fusion cross-sections at low energies for a completely different entrance channel are necessary to

understand the tunneling process at energies well below the barrier.

A new sensitive off-beam-gamma-spectroscopy method to obtain the cross-section of residues from fusion, utilizing a coincidence between characteristic KX-rays and gamma-

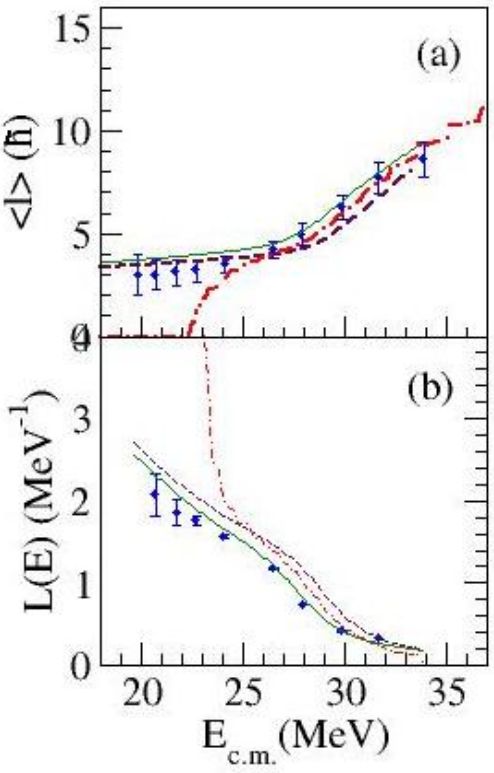

Fig.2 (a) Average angular momentum and (b) logarithmic derivative of the fusion excitation function. The calculated curves are as in Fig. 1.

rays from the daughter nuclei, has been used [5]. This coincidence measurement permitted the accurate and precise determination of the residue cross-sections by reducing the background. The average angular momenta are also presented over the same energy range.

The experiment was performed at Pelletron Linac Facility-Mumbai, using beams of ^{6}Li (5-35 pnA) on a ^{198}Pt target in the range of 20 to 35 MeV. The targets were self supporting rolled foils of ^{198}Pt (95.7% enriched, ~ 1.3~mg/cm^2 thick) followed by an Al catcher foil of thickness ~ 1~mg/cm^2. Two efficiency calibrated HPGe detectors with a Be window and having an active volume ~ 180 cc were placed face to face for performing KX-gamma-ray coincidence of the decay radiations from the irradiated sample. The sample was positioned symmetrically at the center, between the two detectors in a close geometry (1.5 mm from the face of each detector). The measurements were performed in a low background setup with a graded shielding. The reaction products were uniquely identified by means of their characteristic gamma-ray energies and half-lives which in the case of fusion lead to $^{199-202}$Tl residues. The gamma-ray yields of the daughter nuclei were extracted by gating on their KX-ray transitions. Further details of the method can be found in [5]. Due to the increased sensitivity of the KX-gamma-coincidence method, cross-sections down to a few nano-barns could be measured. The fusion cross-sections, obtained from the sum of the measured compound nuclear evaporation residue cross-sections, are plotted in Fig. 1 for ^{6}Li+^{198}Pt. The cross-sections for the sum of deuteron-capture and neutron-transfer (plotted as open squares) are larger than those for fusion by orders of magnitude at deep sub-barrier energies

It has been shown earlier in Ref. [14] that under simple assumptions, the two observables angular momentum (l) and the fusion cross section are not independent, and a model independent relationship exists between the moments of l and the fusion excitation function. As pointed out by Balantekin et al [14], the above does not necessarily imply that the fusion process is governed by an effective one-dimensional energy-independent local potential barrier. In the present work the average angular momenta (<l> have been derived from the fusion excitation function as suggested in [15] and are plotted in Figure. 2a

Calculations using the coupled-channels (CC) code CCFULL were performed with the ingoing-wave-boundary condition. Two sets of calculations, one using a standard Woods-Saxon potential (WS) (V_0=110 MeV, r_0=1.1 fm and a=0.63 fm) and the other based on the M3Y folded potential are presented. The potentials are plotted in Figure. 3. The calculations using the WS potential included the quadrupole excitation

in ^{198}Pt, considering coupling in the vibrational model. For ^{6}Li the 1^{+} (ground state) and the unbound 3^{+} states were assumed to be from a $K^{\pi}= 1^{+}$ rotational band. The results of the calculation with and without the inclusion of the couplings are shown in Figure 1. At energies above the barrier the calculations overestimate the data, as expected from earlier studies involving weakly bound nuclei [16]. As can be seen in the figure, the CC calculations reproduce the data for energies around and well below the barrier. Plotted in Figure 2b is the logarithmic derivative of the fusion cross-section (L(E)=d[ln(σE)]/dE). This representation provides an alternate way to illustrate any deviations in the slope of the fusion excitation function independent of the weight of the lowest barrier. The CC calculations reproduce well both the experimental slope L(E) and the <ℓ> values (Fig.~2(b)) over the entire range of energy. Thus for ^{6}Li + ^{198}Pt, the CC calculations successfully explain the fusion excitation function along with the average angular momentum, consistently implying absence of the fusion hindrance at deep sub-barrier energies.

The lack of the fusion hindrance observed in the present system from the above calculations is also possible if the threshold value for the onset of fusion hindrance was not reached. This is not the case, as shown below. The threshold energy was computed following two independent approaches. The M3Y potential with repulsive core was calculated taking the density distributions of ^{6}Li and ^{198}Pt from [17] and parameters for the repulsive core from Ref.\cite{esb07} (V_{rep} =570 MeV and a_{rep}=0.35 fm, yielding a value of K=220 MeV). The resulting potential (Fig.~3) has a minimum at 21 MeV and as discussed in Refs. [8,10] the threshold energy is larger than this value. Alternatively following the two-step adiabatic model of Ichikawa with Krappe-Nix-Sierk potential [10], the energy at the touching configuration, related to the threshold energy is calculated to be 22.3 MeV (Fig.~3). The present measurements extend down to E_{cm} = 19.8 MeV, which is well below the threshold energy computed from both the approaches.

Single-channel calculations using the above M3Y potential with a repulsive core were also performed as suggested in [11] and the results are shown in Figures 1,2. The calculated fusion cross-sections, for energies lower than 22~MeV, fall off steeply and are orders of magnitude lower than the corresponding single channel calculations using the WS potential (Fig.ure 1). The effect of coupling on the calculated fusion cross-sections are found to be small from the CC calculations as seen in the same figure. A similar behavior was observed in Ref. [16]. Hence at these energies, even including the effect of coupling the calculated fusion cross-sections using the M3Y+repulsive core potential will be much lower than the measured fusion cross-sections. The calculated L(E) values also do not agree with the data and rise more steeply at low energies (Figure 2b). The corresponding mean angular momentum drops to zero around an energy of E=22 MeV which is also inconsistent with the experimental data (Fig. 2a).

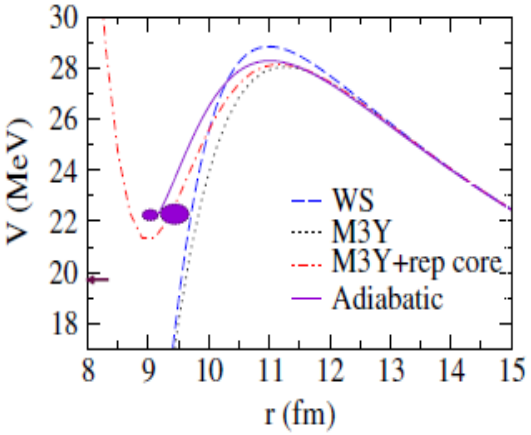

Fig.3 Inter nuclear potentials for ^{6}Li+^{198}Pt using the WS (long dashed line), the M3Y-double folding (dotted line), and the M3Y with a repulsive core (dash-dotted line). The adiabatic potential is shown as a solid curve up to the formation of a neck configuration. The arrow indicates the lowest center of-mass energy where the fusion cross sections were measured

A shallow potential obtained using the M3Y interaction with a repulsive core successfully describe the fusion cross-sections at deep sub-barrier energies for symmetric, asymmetric and positive reaction Q-valued systems [11,13]. But for the present system with a weakly bound

projectile this potential does not reproduce the trend of the fusion excitation function, L(E) and <l>. The present results suggest that the inner part of the interaction potential becomes deeper, going from symmetric to weakly bound asymmetric system, implying reduced contribution of the repulsive core. A plausible reason for this could be as follows: as the nuclei start overlapping, due to the weak binding of one partner, the Fermi energies of the two interacting nuclei are ``very" different and will tend to equilibrate rather fast. Thus the Pauli blocking is expected to be less effective for asymmetric systems involving weakly bound nuclei as compared to two overlapping Fermi levels of symmetric systems [18]. The actual form of the repulsive core is expected to depend also on the extent of the adiabatic nature of the collision [11]. At energies well below the barrier the adiabatic approximation is expected to be more appropriate where nuclear reactions take place following the minimum energy path allowing for the readjustment of the densities as a function of collective variables. The predictions based on the adiabatic model of Ichikawa [10] already appear to give the correct behavior for the average angular momentum in the medium-mass symmetric systems though currently such calculations are not possible for asymmetric systems.

In this section, we have presented the fusion excitation function for very asymmetric system involving weakly bound projectile at energies well below the barrier. This study shows the absence of fusion hindrance, pointing to the limitation of the sudden approximation for modeling reactions in such systems. It would be of interest to see whether this arises solely from the effect of weakly bound cluster structure or also due to difference in transition from the sudden to the adiabatic potential.

3. Sub barrier fusion studies with most neutron rich ^{8}He on ^{197}Au

Both the experimental and theoretical complexities associated with ^{8}He make the study of the tunneling of this nucleus with the largest neutron or proton ratio a challenging problem. In this section we report the first such measurements with reaccelerated beams of ^{8}He

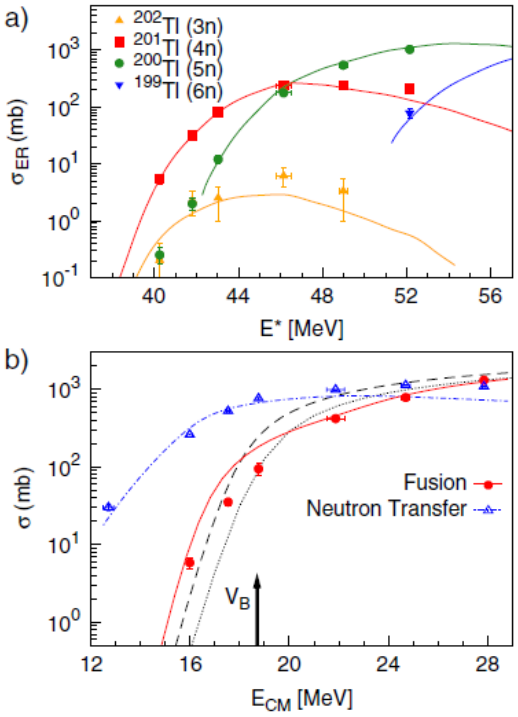

Fig.4 (a) The cross sections for evaporation residues as a function of excitation energy of the compound nucleus. The lines correspond to predictions based on the statistical model code Cascade. (b) Fusion and neutron transfer excitation functions. Two predictions for fusion based on tunneling through a single barrier depending only on the radial separation are shown; dotted line using a nuclear potential derived from a global parameterization; dashed line using a microscopic potential folding the nuclear densities of the target and the projectile. The coupled-channels calculations for fusion and transfer reactions are shown by continuous and dash-dotted lines, respectively. The nominal value of the Coulomb barrier (VB) is indicated.

around the Coulomb barrier. The helium isotopic chain, where the nucleon emission threshold varies from 20.5 MeV to 0.9 MeV, provides unique opportunities for studying the effect of the intrinsic structure on the tunneling process. Both ^{6}He and ^{8}He have ‘‘Borromean’’ structures (removal of the alpha core or one of the neutrons makes the remaining system unbound). Contrary to the general trend, the charge radius of ^{8}He is

smaller than that of ^{6}He due to the more isotropic distribution.

The RIB of ^{8}He ($T_{1/2}$ = 119.1 ms) were produced by fragmentation of a 75 MeV/nucleon ^{13}C beam on a thick graphite target, then fully purified and reaccelerated by the CIME cyclotron at the SPIRAL facility at GANIL. The ^{8}He beam, with an energy resolution better than 2 X 10^{-3} and a beam spot size of ~5 mm diameter and an average intensity of 4 X 10^{5} particles/s, bombarded a stack of ^{197}Au targets. The target stacks consisted of two or three Au targets (~6 mg/cm^2 thick) separated by Al foils (~1 mg/cm^2 thick) to collect recoiling residues and Al foils (from 2 to 10 mg/cm^2 thick) to degrade the beam energy. The different target stacks were irradiated at energies of 2.34, 2.51 and 3:68 MeV/nucleon for 150 h, 24 h and 32 h, respectively. The intensity of the ^{8}He beam was measured using a microchannel plate and a plastic scintillator (10 X 10 X 0.05 cm) placed, respectively, 10 cm upstream and 5 cm downstream with respect to the target. Their time-stamped energy and time signals, correlated with the cyclotron frequency, were used to measure the ^{8}He beam intensity and its time variation during the irradiation. The incident beam energy on the successive target foils was determined based on the energy loss for the Al and Au foils using SRIM [19].

Various reactions can take place: fusion, neutron transfer, direct breakup and elastic scattering of the projectile. The $^{199–202}$Tl nuclei, arising after the evaporation of neutrons from the compound nucleus ^{205}Tl, were characterized by their radioactive decay. These off-beam measurements were made using two lead-shielded detector setups, the first optimized for x-gamma coincidences and the second consisting of two clover detectors to maximize the x-ray detection efficiency. Absolute photo-peak efficiencies of the above two setups were obtained using complete GEANT4 [20] simulations which reproduced within 4% the results of measurements made with five calibration sources (including a ^{201}Tl source) at various distances. Unambiguous identification of the energy and time of disintegration was obtained using a new sensitive and accurate off-beam coincidence technique specialized for the measurement of absolute evaporation residue

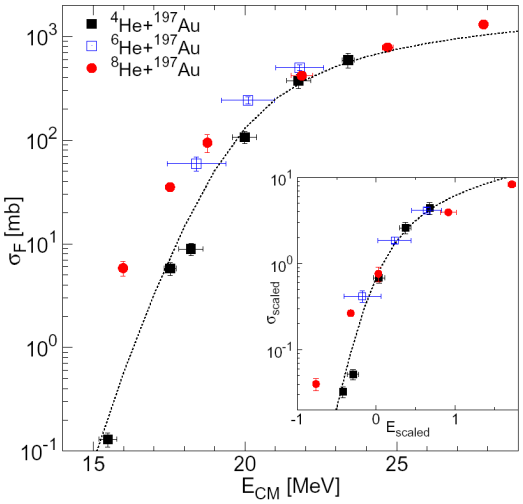

Fig.5 Measured fusion cross section as a function of center-of-mass energy (ECM) for ^{4,6,8}He + ^{197}Au systems. The dotted line shows the one-dimensional barrier penetration calculation for ^{4}He + ^{197}Au obtained using a global parameterization for the nuclear potential. The inset shows suitably scaled cross sections and energies.

cross sections involving low intensity RIB. This method, applied earlier to high intensity stable beams, involves the simultaneous measurement of x and gamma rays emitted in electron capture decays. The final gain in sensitivity, compared to an inclusive experiment, was found to be ~3 X 10^{4}, yielding the first complete and most accurate (having the same quality as for stable beams) fusion cross sections ever measured with reaccelerated RIB. The smallest cross sections measured here (Fig. 4) using reaccelerated RIB are comparable to the current measurement limits in nuclear physics, when scaled by the million times larger intensities available with stable beams. Shown in Fig. 4(a) are the measured individual fusion evaporation residue cross sections, σ_{ER}, as a function of the excitation energy together with predictions of Bohr's model of the statistical decay of an equilibrated compound nucleus [21]. The excellent agreement between the measured σ_{ER} and the calculations confirms that the residues arise from the complete fusion of ^{8}He and ^{197}Au.

The fusion cross section, σ_F, obtained from the sum of the σ_{ER}, is shown in Fig. 4(b). The residues (isotopes of gold) formed after transfer of neutron(s) from the projectile were identified and their activity obtained using inclusive gamma-ray measurements. The total transfer cross section, σ_n, obtained from the sum of the cross sections for ^{198,198m,199}Au residues is also shown. Figure 4(b) also shows the calculated fusion cross sections for tunneling through a single barrier, depending only on the internuclear distance, calculated with a nuclear potential derived either from a global parameterization [22] (dotted) or from a microscopic double-folded potential using realistic densities (dashed). The difference between the two calculations demonstrates the effect of the extended neutron distribution of the ^{8}He nucleus. The dramatic decrease in the measured fusion cross section for energies at and above the barrier, along with a modest increase below the barrier (with respect to the dashed line) can be observed from the figure. The dominance of the transfer processes is seen from the magnitude of the measured σ_n that are much larger than σ_F even at energies well above the barrier. Coupled-channels calculations [23] using the code FRESCO [24] were performed to understand the influence of the direct, one-step transfer channels ^{197}Au (^{8}He, 6,7He)^{199,198}Au on the fusion process. The 1n-transfer calculations were made ignoring the spin of the ^{197}Au core (to keep them tractable) with appropriate single-particle states and spectroscopic factors. For the 2n transfer, based on semiclassical Q-matching conditions [22], transitions to states above the 1n-emission threshold but below that for 2n emission for ^{199}Au were included. A pure 2n + ^{197}Au cluster structure with cluster-core relative angular momentum ranging from 0 to 5 hbar was considered. The distorting potentials in the entrance and exit channels consisted of double-folded real and short-ranged imaginary parts. The observed behavior of the fusion excitation function is reproduced by these coupled-channels calculations (continuous line) including coupling to the transfer channels (dash-dotted line). The good agreement of the calculations including only neutron transfer channels shows that the low particle threshold (2.1 MeV) does not imply a crucial influence of breakup of the projectile on the tunneling process, as is generally assumed for weakly bound nuclei (see Ref. [25] for a recent spectroscopic study of ^{8}He). The role of pairing correlations which stabilize ^{8}He and result in an enhancement of the neutron-pair transfer over single neutron transfer was also shown by the present calculations.

Figure 5 shows the measured fusion cross sections for helium isotopes with ^{197}Au. The good agreement between the calculated and measured fusion cross section for ^{4}He reiterates its point like behavior. At energies below the barrier, σ_F for ^{8}He and ^{6}He [26] are unusually similar and as expected are larger than for ^{4}He [27]. A loosely bound system with a subsystem that does not feel the barrier can more easily restructure during the dynamical process of fusion, emphasizing the role of a flexible intrinsic wave function that can adiabatically readjust in a slow process and increase penetration

Understanding the intriguing behavior of the helium isotopes will influence future applications towards the production of superheavy elements [29] and the study of decoherence effects in open quantum systems [30].

4. Incomplete fusion in ^{7}Li + ^{198}Pt

Recent exclusive measurements of outgoing fragments either after breakup or transfer followed by breakup of ejectile with ^{6,7}Li and ^{9}Be have provided valuable insight on non-capture breakup processes with weakly bound projectiles [31-35]. Alternatively by using particle-gamma coincidence method in case of ^{6}Li(^{7}Li), deuteron (triton) capture have been suggested to be from the process of breakup fusion [36-38]. This work is aimed to study the capture reaction for the well known alpha and t clusters in ^{7}Li and identify the process of capture/transfer of the heavy fragment ^{6}He.

Measurements of particle-gamma coincidences are presented to study the mechanism of different fragment capture/transfer reactions (alpha, t, ^{6}He) leading to unbound final states. The experiment was performed at ^{7}Li beam energies of 29 and 45~MeV, incident on a 1.3 mg/cm^2 thick foil of ^{198}Pt. Four

telescopes (ΔE~25-30μm and E~1mm) at 50^0 60^0, 120^0 and 130^0 (covering the region around and away from the grazing angle) were used to measure the charged particles produced. Four efficiency calibrated and Compton suppressed clover detectors, to record the coincident gamma-rays, were placed at 14.3 cm from the target position at angles of -55^0, 35^0, 80^0, and 155^0. A fast coincidence between any charged particle detected in the ΔE and gamma-rays in any clover detector or a twofold gamma-ray coincidence was used as an event trigger.

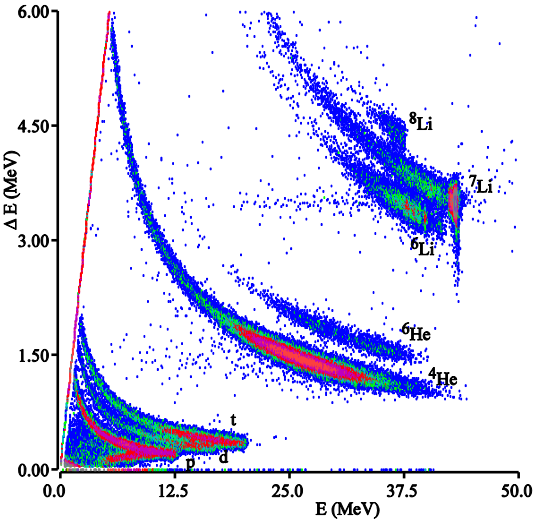

Fig.6 Particle identification plot of energy loss vs total energy obtained in the telescope placed at θ_{lab} 50 degrees for beam energy of 45~MeV. The different reaction products are labeled.

A typical particle identification spectrum for the telescope at forward angle (50^0) is shown in Fig. 6. Plotted in Figs. 7,8 is the add-back gamma-ray spectra from the clover detectors generated by selecting outgoing particles detected in telescopes near the grazing angle (50^0 and 60^0) at the beam energy of 45 MeV. The reaction products arising from different channels could be identified by their characteristic gamma-ray transitions. Only the true-prompt events from the time to amplitude converter spectra of the particle-gamma-ray coincidence were considered. By selecting t-gate, gamma-transitions from residues (^{199,200}Hg) formed after alpha-capture are seen as labeled in Fig. 7. The high-spin states up to 12^- and 14^+ respectively for negative and positive parity yrast-levels in ^{200}Hg are observed as reported in Ref. [39] for alpha + ^{198}Pt. The gamma-transitions populating the isomeric state ($13/2^+$, T1/2~ 42.8~min) in ^{199}Hg have relative intensities of gamma-rays similar to the spectra observed with alpha beam on ^{198}Pt [40].

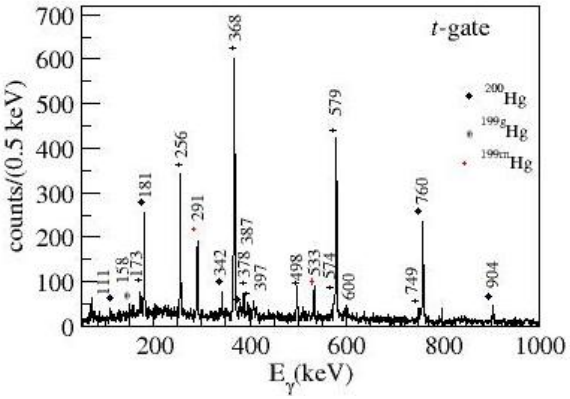

Fig.7 Prompt gamma ray spectra for E_{lab}=45 MeV obtained in coincidence with outgoing triton.

In Fig. 8 (top panel), contribution from different reaction channels can be seen with the alpha gate. The major part of the spectrum is due to residues from t-capture (^{198,199}Au). In case of ^{198}Au, the observed gamma-ray transitions from the levels below the isomeric state at 12^- [41] are labeled. Fig. 8 (bottom panel) shows relatively smaller yield of gamma-rays from ^{198,199}Au due to one proton transfer reaction obtained by selecting the scattered ^{6}He. Both ^{198}Au and ^{199}Au have isomeric states that result in overall loss of the measured yield. The gamma-lines due to 1n and 2n-transfer, arising from ^{199}Pt, ^{200}Pt are also present in the gamma-ray spectrum with the alpha-gate .

The residues from proton pick-up channel could not be detected due to presence of isomeric states in ^{197}Ir. For this nucleus, transitions reported in literature below these states could not be seen and information on transitions from states above the isomeric states is not available. The statistics in the particle-gated gamma-spectra at 29 MeV was limited. At this energy, gamma-lines from ^{200}Hg with t-gate (transitions

up to 6^+ state) and from ^{199}Au with alpha-gate were observed. The results from ^{6}He capture will be presented.

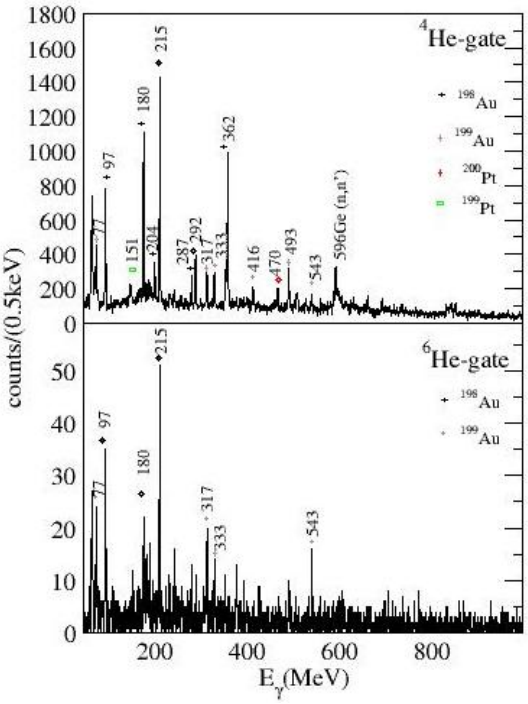

Fig.8 Prompt gamma ray spectra for E_{lab}=45 MeV obtained in coincidence with outgoing alpha (top panel) and ^{6}He (bottom panel)

Acknowledgments

The author would like to thank all the collaborators for useful discussions while preparing this manuscript

References

[1] A.B. Balantekin, N. Takigawa, Rev. Mod. Phys. 70, 78 (1998), M. Dasgupta et al., Ann. Rev. Nucl. Sci. 48, 401 (1998).
[2] C.L. Jiang et al., Phys. Rev. Lett. 89 052701 (2002).
[3] LF. Canto et al, J. Phys. G 36, 015109 (2009)
[4] C. Palshetkar et al Phys. Rev. C 82, 044608 (2010) and references therein.
[5] A. Lemasson et al., Nucl. Instrum. Methods Phys. Res.,Sect. A 598, 445 (2009).
[6] A. Lemasson et al , Phys. Rev. Letts.103, 232701 (2009) .
[7] A. Shrivastava et al, Phys. Rev. Letts. 103, 232702 (2009).
[8] C. H. Dasso and G. Pollarolo, Phys. Rev. C 68, 054604 (2003).
[9] K. Hagino and Y. Watanabe, Phys. Rev. C 76, 021601(R) (2007),
[10] T. Ichikawa, K. Hagino, and A. Iwamoto, Phys. Rev. C 75, 064612 (2007).
[11] S. Mis¸icu and H. Esbensen, Phys. Rev. Lett. 96, 112701 (2006); Phys. Rev. C 75, 034606 (2007).
[12] M. Dasgupta et al., Phys. Rev. Lett. 99, 192701 (2007)
[13] H. Esbensen and S. Mis¸icu, Phys. Rev. C 76, 054609 (2007).
[14] A. B. Balantekin and P. E. Reimer, Phys. Rev. C 33, 379 (1986).
[15] C.V. K. Baba, Nucl. Phys. A553, 719 (1993); V. Tripathi et al., Phys. Rev. Lett. 88, 172701 (2002).
[16] M. Dasgupta et al., Phys. Rev. C 66, 041602(R) (2002).
[17] L. C. Chamon et al., Phys. Rev. C 66, 014610 (2002).
[18] D. Lacroix, Macroscopic Approaches for Fusion Reactions (Ecole Joliot-Curie, Maubuisson, 2002) available at http://www.cenbg.in2p3.fr/heberge/EcoleJoliotCurie/ coursJC/JOLIOT-CURIE2002.pdf.
[19] J. F. Ziegler, The Stopping and Range of Ions in Matter, http://www.srim.org/.
[20] S. Agostinelli et al., Nucl. Instrum. Methods Phys. Res.,Sect. A 506, 250 (2003).
[21] F. Pu¨lhofer, Nucl. Phys. A 280, 267 (1977).
[22] R. A. Broglia and A. Winther, Heavy Ion Reactions, Frontiers in Physics Lecture Note Series Vol. 84 (Addison-Wesley, Redwood City, CA, 1991).
[23] N. Keeley, N. Alamanos, K.W. Kemper, and K. Rusek,Prog. Part. Nucl. Phys. 63, 396 (2009).
[24] I. J. Thomson, Comput. Phys. Rep. 7, 167 (1988).
[25] M. S. Golovkov et al., Phys. Lett. B 672, 22 (2009).

[26] Yu. E. Penionzhkevich et al., Eur. Phys. J. A 31, 185 (2007).
[27] M. S. Basunia, H. A. Shugart, A. R. Smith, and E. B.Norman, Phys. Rev. C 75, 015802 (2007).
[28] A. Sakharuk, V. Zelevinsky, and V. G. Neudatchin, Phys.Rev. C 60, 014605 (1999).
[29] Y. Aritomo, Phys. Rev. C 75, 024602 (2007).
[30] N. D. Antunes, F. C. Lombardo, D. Monteoliva, and P. I.Villar, Phys. Rev. E 73, 066105 (2006).
[31] A. Shrivastava it et al. Phys. Letts. B 633, 463 (2006).}
[32] S. Santra it et al., Phys. Letts. B 677, 139 (2009).
[33] R. Rafiei it et al., Phys. Rev. C 81, 024601 (2010).
[34] A. Pakou it et al., Phys. Letts. B 633, 691 (2006).
[35] T.A.D. Brown it et al., Phys. Rev. C 76, 054605 (2007).
[36] V.Tripathi it et al., Phys. Rev. C 72, 0170601 (2005).
[37] C.M. Castaneda it et al., Phys. Letts. B 77, 371 (1978).
[38] H. Utsunomiya it et al., Phys. Rev. C 28, 1975 (1983).
[39] H. Helppi et al, Phys. Rev. C 23, 2345 (1981).
[40] D. Mertin et al., Nucl. Phys. A 301, 365 (1978).
[41] H.-E. Mahnke, G.Kaindl, F. Bacon and D. Shirley, Nucl. Phys. A 247, 195 (1975).